Acta Pharmaceutica Sinica B 2020;10(11):2171–2182

Chinese Pharmaceutical Association
Institute of Materia Medica, Chinese Academy of Medical Sciences

Acta Pharmaceutica Sinica B

www.elsevier.com/locate/apsb
www.sciencedirect.com

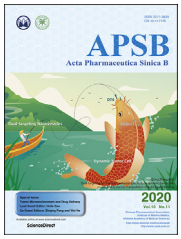

ORIGINAL ARTICLE

Precise delivery of obeticholic acid *via* nanoapproach for triggering natural killer T cell-mediated liver cancer immunotherapy

Guofeng Ji[a,b], Lushun Ma[a], Haochen Yao[b,d], Sheng Ma[b,g], Xinghui Si[b], Yalin Wang[b,e], Xin Bao[b,f], Lili Ma[b,g], Fangfang Chen[a,h], Chong Ma[a], Leaf Huang[c], Xuedong Fang[a,h,*], Wantong Song[b,g,*]

[a]*Department of Gastrointestinal and Colorectal Surgery, China-Japan Union Hospital of Jilin University, Changchun 130033, China*
[b]*Key Laboratory of Polymer Ecomaterials, Changchun Institute of Applied Chemistry, Chinese Academy of Sciences, Changchun 130022, China*
[c]*Division of Pharmacoengineering and Molecular Pharmaceutics, Eshelman School of Pharmacy, University of North Carolina at Chapel Hill, Chapel Hill, NC 27599, USA*
[d]*Key Laboratory of Zoonosis, Chinese Ministry of Education, College of Basic Medical Science, Jilin University, Changchun 130021, China*
[e]*Second Hospital of Shandong University, Jinan 250000, China*
[f]*Second Hospital of Jilin University, Changchun 130041, China*
[g]*Jilin Biomedical Polymers Engineering Laboratory, Changchun 130022, China*
[h]*State Key Laboratory of Inorganic Synthesis and Preparative Chemistry, College of Chemistry, Jilin University, Changchun 130012, China*

Received 25 July 2020; received in revised form 29 August 2020; accepted 1 September 2020

Abbreviations: ALT, alanine aminotransferase; AST, aspartate aminotransferase; BUN, blood urea nitrogen; CDCA, chenodeoxycholic acid; Cr, creatinine; FXR, farnesoid X receptor; H&E, hematoxylin and eosin; HCC, hepatocellular carcinoma; HPLC, high-performance liquid chromatography; HSCs, hepatic stellate cells; IFN-γ, interferon-γ; IVIS, *in vivo* imaging system; LSECs, liver sinusoidal endothelial cells; NE, nanoemulsion; NKT cells, natural killer T cells; OCA, obeticholic acid; PBC, primary biliary cholangitis; TACE, transarterial chemoembolisation; TSR, tumor suppression rate.

*Corresponding authors.
E-mail addresses: fangxuedong@medmail.com.cn (Xuedong Fang), wtsong@ciac.ac.cn (Wantong Song).

Peer review under responsibility of Chinese Pharmaceutical Association and Institute of Materia Medica, Chinese Academy of Medical Sciences.

https://doi.org/10.1016/j.apsb.2020.09.004

KEY WORDS

Obeticholic acid;
Farnesoid X receptor;
Nanoemulsion;
Liver sinusoidal endothelial cells;
Liver cancer

Abstract Primary bile acids were reported to augment secretion of chemokine (C–X–C motif) ligand 16 (CXCL16) from liver sinusoidal endothelial cells (LSECs) and trigger natural killer T (NKT) cell-based immunotherapy for liver cancer. However, abundant expression of receptors for primary bile acids across the gastrointestinal tract overwhelms the possibility of using agonists against these receptors for liver cancer control. Taking advantage of the intrinsic property of LSECs in capturing circulating nanoparticles in the circulation, we proposed a strategy using nanoemulsion-loaded obeticholic acid (OCA), a clinically approved selective farnesoid X receptor (FXR) agonist, for precisely manipulating LSECs for triggering NKT cell-mediated liver cancer immunotherapy. The OCA-nanoemulsion (OCA-NE) was prepared *via* ultrasonic emulsification method, with a diameter of 184 nm and good stability. *In vivo* biodistribution studies confirmed that the injected OCA-NE mainly accumulated in the liver and especially in LSECs and Kupffer cells. As a result, OCA-NE treatment significantly suppressed hepatic tumor growth in a murine orthotopic H22 tumor model, which performed much better than oral medication of free OCA. Immunologic analysis revealed that the OCA-NE resulted in augmented secretion of CXCL16 and IFN-γ, as well as increased NKT cell populations inside the tumor. Overall, our research provides a new evidence for the antitumor effect of receptors for primary bile acids, and should inspire using nanotechnology for precisely manipulating LSECs for liver cancer therapy

1. Introduction

Primary liver cancer is the sixth most common cancer and ranked the fourth major leading cause of cancer-related death worldwide in 2018[1]. With about 840,000 new cases and 780,000 deaths per year, China accounts for over 50% of all the cases[2,3]. Hepatocellular carcinoma (HCC) comprises approximately 80%−90% of primary liver cancer cases[4]. Surgery is the primary therapeutic option for early-stage HCC, however, early-stage HCC only accounts for 5%−10% of all HCC cases[5,6]. For intermediate and advanced stage HCC, due to the existence of local or portal vein invasion at the time of diagnosis, the 5-year survival rate drops dramatically to only 11% and 3%, respectively[7,8]. Transarterial chemoembolization (TACE) and sorafenib are standard clinical therapeutic options against intermediate and advanced stage HCC[9,10]. While overcoming the defects of systemic chemotherapy, TACE could stimulate revascularisation and promote metastasis by aggravating tumor hypoxia and upregulating the expression of vascular endothelial growth factor (VEGF)[11]. Sorafenib was approved by the U.S. Food and Drug Administration (FDA) for the treatment of unresectable HCC in 2007, however, the overall outcomes of sorafenib are far from satisfactory. Sorafenib prolonged the median overall survival time and radiological progression of HCC patients by only 3−5 months[12,13]. Moreover, the use of sorafenib has been hampered by serious adverse side effects, primary and acquired resistance[13].

Cancer immunotherapy, which could trigger the robust systemic antitumor immunity, present significant advantages for cancer therapy over the past several years[14,15]. Liver is a peripheral immune organ that is heavily populated by innate and adaptive immune cells[16]. Therefore, there are great interests in mobilizing the immune cells for liver cancer control[17]. Recently, programmed death-1 antibodies nivolumab and camrelizumab were approved to treat advanced HCC previously treated with sorafenib[18,19], announcing the success of immunotherapy in liver cancer therapy. Besides T cells, liver differences from other organs in that liver lymphocytes are enriched with natural killer (NK) cells and natural killer T (NKT) cells. Specially, NKT cell is a subset of lymphocytes at the interface between innate and adaptive immunity. NKT cells make up 20%−35% and 10%−15% of liver lymphocytes in mouse and human, respectively[20]. NKT cell was demonstrated to actively protect the liver and contributes to antitumor activity and immunity *via* tumor-related cytokines in the liver[21]. Therefore, mobilizing the antitumor immunity of NKT cells in the liver is an attractive research direction for liver cancer management.

The gut–liver axis regulates the metabolism and immune homeostasis in both the gut and the liver[22]. Plenty of studies prove that various metabolites, hormones, and bacterial products transported through the portal vein from the gut to the liver have direct influence on the progress of liver diseases as well as the liver cancer[23,24]. Recently, Ma et al.[25] reported that the gut-recovered bile acid had direct influence on the NKT cell recruitment into the liver. Specifically, primary bile acids augment secretion of chemokine (C–X–C motif) ligand 16 (CXCL16) from liver sinusoidal endothelial cells (LSECs) and trigger robust NKT cell-based immunotherapy for liver cancer through the recruitment of NKT cells to the liver; while secondary bile acids function on the opposite way. This study reveals the gut microbiota uses bile acids as messengers to mediate the antitumor immunity in the liver, and provides possible implications for interfering the gut–liver bile acid pathway for liver cancer immunotherapy.

Liver-derived primary bile acids are transformed into secondary bile acids in the gut by microbiota through deconjugation and dehydroxylation reaction[26]. While direct manipulating the gut microbiota is complicated, using selective agonists against receptors for primary bile acids or antagonists against receptors for secondary bile acids may bypass the microbiota and directly target LSECs for recruiting NKT cells into the liver. Antagonists against receptors for secondary bile acid are seldom and not available for clinical application at present. Currently, there are many receptor agonists for primary bile acid on the market. Among them,

obeticholic acid (OCA) was reported to have high activity over others in interacting with the farnesoid-X receptor (FXR), and has been approved by FDA and European Agency for the Evaluation of Medicinal Products (EMEA) as an orphan drug for the therapy of primary biliary cholangitis (PBC)[27]. However, due to the abundant expression of FXRs in the gastrointestinal tract, direct usage of OCA results in low availability to the liver, while high dosing of OCA could result in high incidence of severe adverse effects, which is dose-dependent[28]. In September 2017, FDA issued a warning for patients treated with OCA. Inappropriately high dosing of OCA results in serious liver injury and death[29]. LSECs have been validated as the major source of CXCL16 in the liver after stimulating with primary bile acids[30]. Interestingly, LSECs together with Kupffer cells constitutes the major cells in the liver for capturing and clearing nanoparticles from the blood circulation[31]. This intrinsic property makes delivery of OCA with a nanoapproach an ideal way for precise manipulating LSECs for recruiting NKT cells and inhibiting tumor growth in the liver[32]. Given this background, we tested a nanoemulsion (NE) formulation of OCA for triggering NKT cell-based immunotherapy for liver cancer in this study (Scheme 1).

2. Material and methods

2.1. Chemicals and reagents

Obeticholic acid (OCA) was bought from Chemlin Chemical Industry Co., Ltd. (Nanjing, China). Lecithin was purchased from TCI (Tokyo, Japan). Poloxamer 188 solution (Pluronic® F-68 solution) was bought from Sigma−Aldrich (St. Louis, MO, USA). IFN-γ and CXCL16 ELISA kit were purchased from Anrc Bio. Tech. (Tianjin, China). 1,1′-Dioctadecyl-3,3,3′,3′-tetramethylindodicarbocyanine perchlorate (DiD) was obtained from Solarbio Science & Technology Co., Ltd. (Beijing, China). Antibodies (Supporting Information Table S1) were bought from BD Biosciences (Franklin Lakes, NJ, USA) and BioLegend (San Diego, CA, USA).

2.2. Preparation and characterization of NE

Blank NE or NE loaded with OCA or DiD were prepared by an ultrasonic emulsification method. In brief, 20 mg OCA or 0.2 mg DiD was dissolved in 200 μL dimethyl sulfoxide (DMSO), which was then added with 250 μL olive oil and 100 mg lecithin from soybean. The mixture was stirred for 3 min at room temperature. Next, 1 mL pluronic® F-68 solution was slowly added into the above mixture with a gentle stirring and continually stirred for 20 min. The mixture was then emulsified by probe sonication (350 W) for 20 min on ice bath to produce NE. Next, the NE was diluted with Milli-Q water (Milli-Q Advantage, MA, USA) to liquid with a final concentration.

2.3. In vitro drug release

The *in vitro* release profiles of OCA from OCA-NE were tested using dialysis tube. 5 mL OCA-NE solution (1.1 mg/mL) were added to dialysis tubes (MWCO 7000 Da). Then the dialysis tubes were transferred into 40 mL phosphate buffered saline (PBS) solution (pH 7.4 and 6.5) with 0.2% (*w*/*v*) Tween 80. The dialysis tubes were placed into a 37 °C shaking box (100 rpm, HZQ-X100, Harbin, China) in dark for 48 h. At predetermined time points (0.5, 2, 4, 6, 8, 12, 24 and 48 h), 4 mL release solution was collected and replaced with 4 mL same fresh buffer. The OCA concentrations were determined by high-performance liquid chromatography (HPLC, PerkinElmer Flexar™, Waltham, MA, USA). The HPLC equipped with an InertSustain C18 column (250 mm × 4.6 mm × 5 μm, 5020-07346), and the mobile phase consisted of water and acetonitrile (20:80; flow rate: 1 mL/min; wavelength: 195 nm).

2.4. Cell lines and animals

The mouse hepatic cancer cell line, H22 were obtained from the BeNa Culture Collection (Beijing, China). Mouse 3T3 fibroblasts were bought from the BeNa Culture Collection (Beijing, China). Mouse 3T3 fibroblasts were cultured with Dulbecco's modified Eagle's medium (DMEM), which contains 10% fetal bovine serum (FBS), 50 U/mL penicillin and 50 U/mL streptomycin, and incubated at 37 °C in an atmosphere of 5% CO_2.

Healthy BALB/c mice (female, 8 weeks old, 18–20 g), Kunming mice (KM mice, female, 8 weeks old, 20–25 g) and SD rats (female, 7 weeks old, 200–220 g) were bought from Beijing Vital River Laboratory Animal Technology Co., Ltd. (Beijing, China). All mice were separately raised and used according to the guidelines on Laboratory Animals of Jilin University (Jilin, China). Animal room were kept on constant temperature (20–22 °C) and relative humidity (55%).

For H22 orthotopic liver cancer model establishment, healthy female BALB/c mice were narcotized routinely with isoflurane and fixed on an operation table. The abdominal skin was disinfected with complexing iodophors, and a 1 cm incision was made in the middle of abdomen to expose liver. H22 cells obtained from the ascites of KM mice were washed with PBS and diluted into a concentration of 2×10^7 cells/mL, and 5×10^5 cells (25 μL) were slowly injected into the left lobe of the liver, and syringe pinhole was coagulated with electrotome immediately to prevent tumor cells from leaking into the abdominal cavity. In the end, the small incision was sewn up with 5-0 silk line and disinfected with 75% ethanol. The mice were kept warm and monitored carefully until conscious.

2.5. Cytotoxicity assay in vitro

The cytotoxicity of OCA and OCA-NE were determined by MTT assay. The mouse H22 cells or 3T3 fibroblast were seeded in the 96-well plates (8000 cells per well) and cultured overnight with 180 μL RPMI 1640 or DMEM, then 20 μL PBS with scheduled concentration of free OCA and OCA-NE (0.001–100 μg/mL) were added and incubated for another 24 or 48 h. At determined time points, 20 μL MTT reagents were added into the plates followed by 4 h incubation. The absorbance was determined using a microplate reader at 490 nm. The cell viability (%) was displayed as the percentage of treated cells *versus* untreated control cells.

2.6. Pharmacokinetics study

For the pharmacokinetic study, healthy female SD rats (average weight 200 g, 4 mice/group) received OCA-NE (20 mg/kg i.v.) or free OCA (20 mg/kg *p.o.*). Approximately 300 μL of blood samples were collected from orbit sinus at pre-established intervals during 24 h (0.5, 1, 2, 4, 6, 8, 12, and 24 h). The blood samples were centrifuged at 4 °C to obtain supernatant plasma,

and equal volumes of 1 mol/L hydrochloric acid and 1.2 mol/L disodium hydrogen phosphate were added to each sample. Then the samples were centrifuged at 4 °C and the supernatant was collected and filtered through 0.22 μm filters for HPLC analysis. The pharmacokinetic data was analysed by Data and max Statistics (DAS, Shanghai, China).

2.7. *In vivo and cellular biodistribution of OCA-NE*

150 μL of DiD-encapsulated NE (67 μg/mL, representing OCA-NE) were intravenously injected into healthy female BALB/c mice *via* tail vein. After 4 or 24 h, mice were sacrificed and immediately received cardiac perfusion with PBS and their major organs were collected. The fluorescence imaging of major organs was conducted to investigate *in vivo* biodistribution of OCA-NE.

To analyze the distribution of DiD-NE at cellular level, the perfused liver processed into single cell suspensions 4 h after injection of OCA-NE. Then extracted single cell suspensions were stained with fluorophore-conjugated antibodies and then detected by flow cytometry. The single liver cells were identified according to the following markers: hepatocytes (large $CD146^-$ $F4/80^-$ cells), LSECs ($CD146^+$ $F4/80^-$ cells), Kupffer cells ($CD146^-$ $F4/80^+$ cells), and other liver cells (small $CD146^-$ $F4/80^-$ cells) including HSCs, B cells, and others.

2.8. *Biodistribution study in tumor-bearing mice*

The *in vivo* biodistribution of OCA-NE and OCA in the liver tissue and the orthotopic tumor were assessed in H22 tumor-bearing mice. Female H22 tumor-bearing BALB/c mice (female, 8 weeks old, 18–20 g, 7 days after tumor inoculation) received OCA-NE (20 mg/kg, i.v.) or OCA (20 mg/kg, *p.o.*). The liver tissues and tumors were excised at predetermined time points (4 and 24 h), accurately weighed and grind into pieces. The tissue debris was treated with 1 mol/L hydrochloric acid and 1.2 mol/L disodium hydrogen phosphate. Finally, the obtain supernatant was detected by HPLC.

2.9. *Murine orthotopic H22 liver cancer therapy*

At three days after tumor inoculation, the mice were divided randomly into four groups, and treated with PBS (i.v.), OCA (20 mg/kg, *p.o.*), blank NE (i.v.), OCA-NE (20 mg/kg, OCA equivalent, i.v.). The treatment schedule was three times per week for 2 weeks. The tumor and liver weight were dissected and recorded at the end of the experiment. Tumor suppression rate (TSR, %) was calculated as following Eq. (1):

$$\mathrm{TSR}\,(\%) = [(A_c - A_x)/A_c] \times 100 \quad (1)$$

where A_c and A_x represented the average weight of tumors in the control (PBS) and the treatment (OCA, NE or OCA-NE) groups.

2.10. *Serum biochemical parameters*

Peripheral blood was collected from mice after 2-week of treatment. The concentration of alanine transaminase (ATL) and aspartate transaminase (AST) and the of blood urea nitrogen (BUN) and creatinine (CRE) in the serum were determined with kits according to the instructions and compared.

2.11. *Histological analysis*

Mice were euthanatized at the end of observation. The excised liver tumors were fixed in 4% paraformaldehyde solution, embedded in paraffin and sliced at 5 μm thickness. Then, slices were stained with hematoxylin and eosin (H&E) to examine pathology. Histological photos were observed by light microscopy (IX71, Olympus, Tokyo, Japan).

2.12. *Flow cytometry analysis*

Tumors and spleens were harvested at the end of the experiment. The tumors were cut into small pieces and homogenized with RPMI 1640 containing collagenase IV. Then the supernatant from the digested tumor tissues were collected, filtered, centrifuged and resuspended. The spleen was mechanically grinded, filtered and resuspended in RPMI 1640. Red blood cell lysis buffer was used to lyse erythrocytes. Finally, cell suspensions were stained with the fluorophore-conjugated antibodies, and flow cytometry analysis was performed on a BD FACS Celesta flow cytometer (BD Biosciences).

2.13. *Cytokine analysis*

Peripheral blood and tumor were collected from mice after 2-week of treatment. Tumor tissue (~100 mg) was excised and homogenized in protein extraction buffer containing protease inhibitor (1 μg/mL). Concentrations of IFN-γ and CXCL16 in serum and tumor tissues were then determined by ELISA kit according to the manufacturer's directions. Cytokine concentrations in serum and tumor tissues were presented as pg/mL or pg/g of protein, respectively.

2.14. *Statistical analysis*

Two-tailed unpaired Student's *t*-test was conducted for comparison of 2 treated groups. All results were presented as the mean ± SEM (standard error of mean)/SD (standard deviation). Significance difference is considered when $P < 0.05$ ($^*P < 0.05$, $^{**}P < 0.01$, $^{***}P < 0.001$, $^{****}P < 0.0001$).

3. Results and discussion

3.1. *Preparation and characterization of OCA-NE*

OCA-NE were prepared *via* an ultrasonic emulsification method according to the methods reported in literatures with minor modifications (Fig. 1A)[33,34]. As shown in Fig. 1B, DLS results show that the prepared OCA-NE had uniform size distribution with an average diameter of approximately 184 nm. Typical TEM image indicate that spherical emulsion droplets are formed and the average size was about 200 nm in the dehydrated condition (Fig. 1C), which is in accordance with that obtained from the DLS results. Then the storage stability of the OCA-NE was evaluated. Fresh OCA-NE were tightly sealed and stored for 30 days at 4-degree-Celsius refrigerator. No visible changes in mean diameter and morphology were observed compared with the original fresh formulations (Fig. 1D and E). In addition, no phase separation nor drug precipitation was seen during the observation period. These results validate that OCA-NE were successfully prepared with

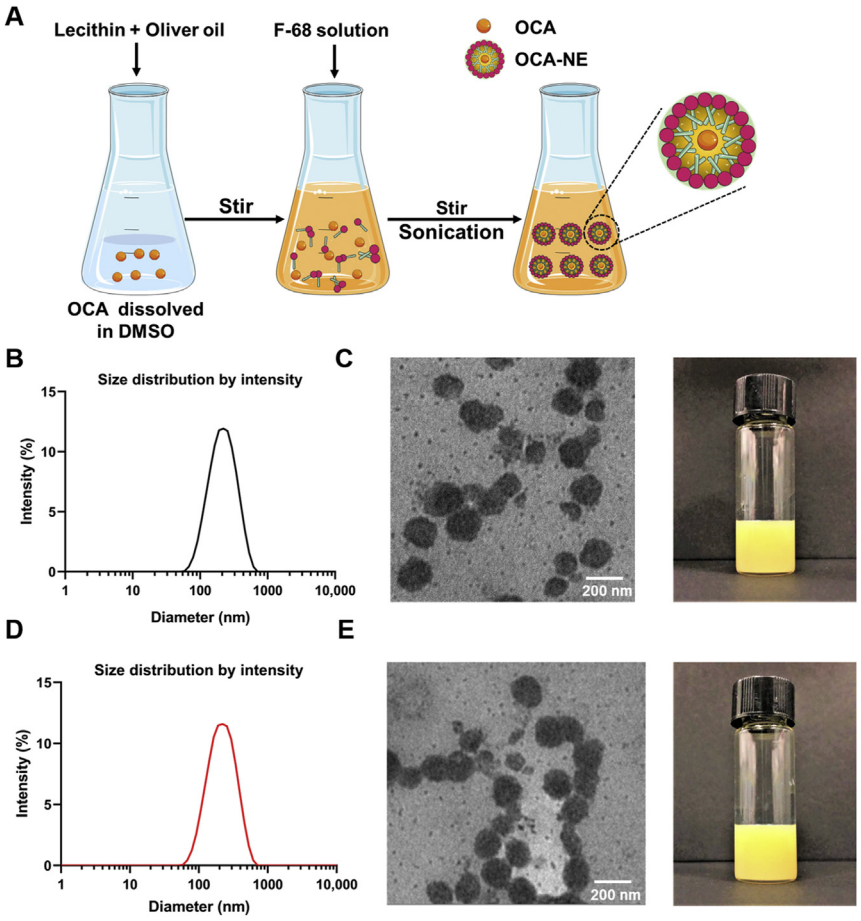

Figure 1 Preparation and characterization of OCA-NE. (A) Schematic illustration of preparation of OCA-NE *via* an ultrasonic emulsification method. (B) and (C) Hydrodynamic diameters as measured by DLS and representative TEM image and photo of OCA-NE. scale bar = 200 nm. (D) and (E) Hydrodynamic diameters as measured by DLS and representative TEM image and photo of OCA-NE after storage for 1 month; scale bar = 200 nm.

small droplet size (184 nm), uniform size distribution and good stability.

3.2. *In vitro drug release*

In vitro release profiles of OCA from OCA-NE were studied in different PBS solution (pH 7.4 and 6.5). The different PBS solutions were used to represent the normal blood environment (pH 7.4) and tumor extracellular fluid environment (pH 6.5). As shown in Supporting Information Fig. S1, the OCA cumulative release within 24 h at pH 6.5 and 7.4 were 87.2% and 64.8%, respectively. After 48 h of incubation, the release of OCA-NE at pH 6.5 and 7.4 were 93.7% and 73.2%, respectively. The release rate at pH 6.5 is faster than that at pH 7.4, which may be attributed to the less stability of NE at acidic conditions.

3.3. *In vitro cytotoxicity*

Firstly, the cytotoxicity of free OCA and OCA-NE to normal cells was assessed in mouse 3T3 fibroblasts. As shown in Fig. 2A, after incubation for 24 and 48 h, no obvious cytotoxicity was observed even at OCA concentrations of 100 μg/mL. Then the cytotoxicity of the free OCA and OCA-NE were evaluated in H22 tumor cells. MTT assay shows that OCA and OCA-NE decreased the rate of cell proliferation at a high dosage, as compared to the corresponding control (Fig. 2B). The cytotoxicity of OCA or OCA-NE to H22 cells was dose- and time-dependent. The IC_{50} of OCA and OCA-NE to H22 cells at 24 and 48 h are 41.1, 68.3 and 8.9, 4.0 μg/mL, respectively. The mild toxicity of OCA and OCA-NE to H22 cells is similar to previous reports[35,36]. The mechanism in the cytotoxicity of OCA to tumor cells is mainly attributed to interfere with IL-6/Janus kinase 2 (Jak-2)/signal transducer and activator of transcription 3 (STAT3) signalling pathway[35].

3.4. *Pharmacokinetics study*

The pharmacokinetics studies of free OCA (*p.o.*) and OCA-NE (i.v.) were performed in SD rats. As expected, free OCA showed much lower absorption and higher clearance from blood circulation *in vivo* (Fig. 3). In contrast, the designed OCA-NE showed higher bioavailability and extend the blood circulation time ($t_{1/2}$ = 17.5 ± 2.3 h) compared with free OCA ($t_{1/2}$ = 7.6 ± 1.4 h). As shown in Supporting Information Table S2, the $AUC_{0\text{-}t}$ of the OCA-NE in 24 h is 763.4 ± 65.8 μg/mL·h, while the $AUC_{0\text{-}t}$ of free OCA is 387.9 ± 25.9 μg/mL·h. These results evidence that OCA-NE possessed longer half-life and superior bioavailability compared with free OCA.

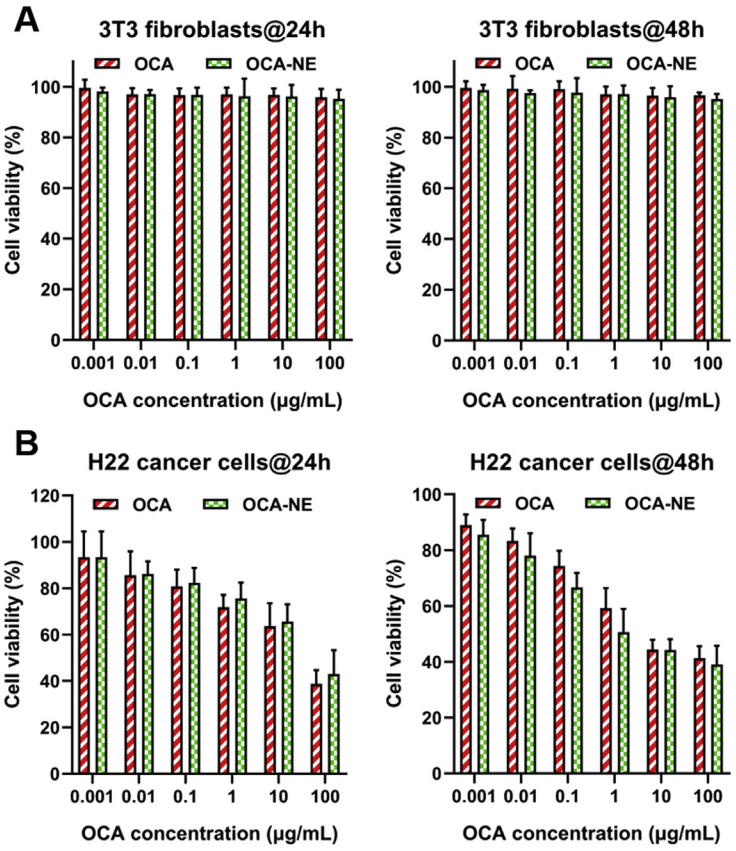

Figure 2 *In vitro* cell viability of mouse 3T3 fibroblasts (A) and H22 cells (B) incubated with free OCA and OCA-NE for 24 and 48 h. Data represent mean ± SD ($n = 4$ for 3T3 fibroblasts, $n = 3$ for H22 cells).

3.5. *In vivo and cellular biodistribution of OCA-NE*

DiD labeling is widely-applied in nanoparticle biodistribution studies owing to the slow release rate of DiD from the nanoparticle[37]. Furthermore, DiD could avoid overlap with endogenous liver-tissue autofluorescence. Thus, DiD was used to assess the *in vivo* biodistribution of the applied NE. The DiD-NE was prepared following a method exactly the same to the OCA-NE, and the obtained NE showed a similar diameter with OCA-NE (Supporting Information Fig. S2). At 4 and 24 h after injection, major organs were excised and fluorescence imaging was conducted in tumor free BALB/c mice (Fig. 4A). Quantitative analysis of the DiD fluorescence intensity was conducted for determining the NE distribution in different tissues. As shown in Fig. 4B and C, DiD-NE displays dominant accumulation in liver over other organs. This is in accordance with common views that liver is the major organ with profound reticuloendothelial system for capturing and clearing nanoparticles from the blood circulation[38]. Furthermore, we excised the liver and analyzed the distribution of DiD-NE at cellular level. Hepatocytes, LSECs, Kupffer cells, and HSCs account for 57%, 23.2%, 15%, 1.8% of the total cells in liver, respectively[39,40]. LSECs line the sinusoidal capillary channels of the liver and are the most abundant non-parenchymal hepatic cell population. Specially, together with Kupffer cells, LSECs constitute the most powerful scavenger system for clearing virus particles or nanoparticles from the circulation[41,42]. Then, we examined the NE distribution by major liver cells with flow cytometry (Gating strategy shown in Supporting Information Fig. S3). As shown in Fig. 4D, approximately 82% of LSECs and 88% of Kupffer cells are DiD-positive, whereas only a small percentage of hepatocytes and other cells in liver are DiD positive. The biodistribution and the cellular distribution results clearly show that LSECs is a major target for the i.v.-injected NE, and thus provide the rationale using nanoapproach for precisely manipulating LSECs for liver disease therapy.

3.6. *Biodistribution study in tumor-bearing mice*

The *in vivo* biodistribution of OCA-NE and OCA in liver tissue and the orthotopic tumor were also assessed. Female BALB/c mice received OCA-NE (20 mg/kg i.v.) or OCA (20 mg/kg *p.o.*).

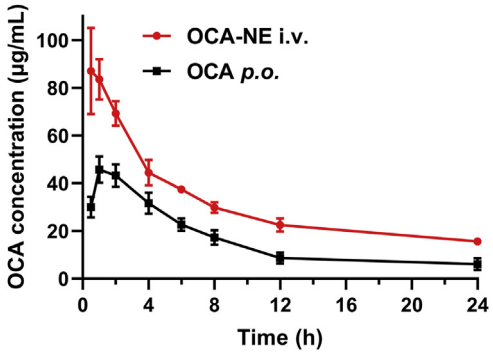

Figure 3 Plasma concentration−time profiles in SD rats treated with free OCA (*p.o.*) and OCA-NE (i.v.) at a dose of 20 mg/kg. Data are mean ± SD ($n = 4$).

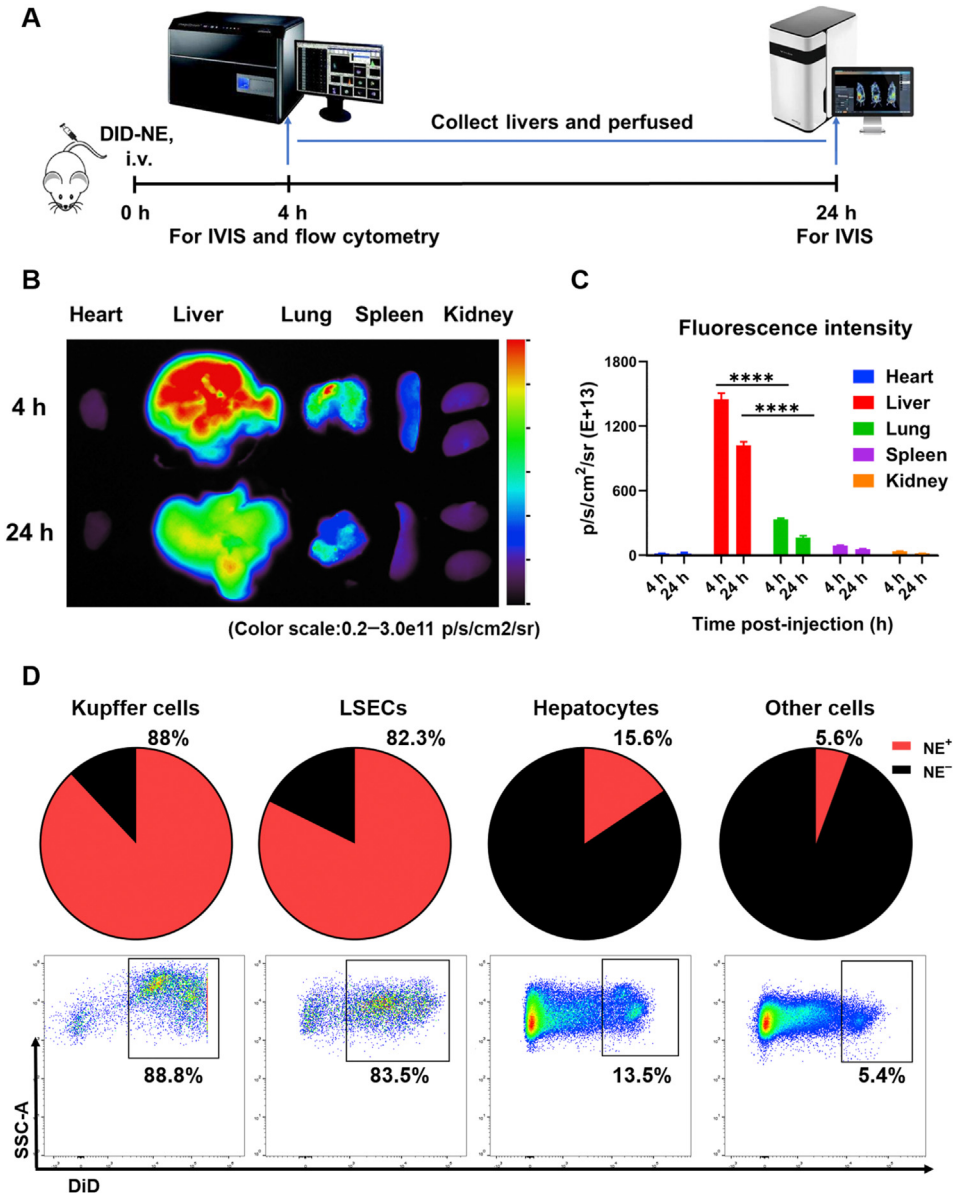

Figure 4 *In vivo* and cellular distribution study of DiD-NE in BALB/c mice. (A) Schematic illustration of the distribution experiment design. The vital organs were perfused and collected at 4 and 24 h for IVIS after i.v. injections of DiD-NE. The livers collected at 4h were also analyzed with flow cytometry to investigate the relative NE uptake by major liver cells. (B) Representative fluorescence images of vital organs captured at 4 and 24 h after i.v. injections of DiD-NE. (C) Fluorescence intensity of vital organs at 4 and 24 h. Data were presented as the mean ± SEM ($n = 3$). (D) Percentage of cells that internalized NE (DiD^+) within hepatocytes, endothelial cells, Kupffer cells, and other cells at 4 h after injection. Data were presented as the mean ± SEM ($n = 8$); ****$P < 0.0001$.

The normal liver tissues and tumors were excised at predetermined time points (4 and 24 h). Then quantitative analysis of the OCA concentration was performed with HPLC for determining the OCA concentration in the liver and tumor. As shown in Supporting Information Fig. S4, the concentration of OCA in the OCA-NE group is higher than that in the free OCA group in both liver and tumor tissues. In addition, the overall concentration in liver tissues is higher than that in the tumor tissues in the OCA-NE group, suggesting the injected OCA-NE was mainly captured in the liver tissue cells.

3.7. *In vivo anti-tumor efficacy of OCA-NE*

The anti-tumor efficacy of OCA-NE was determined on orthotopic HCC mice model which was more clinically relevant[43,44]. The orthotopic liver cancer model was established by directly injecting 5×10^5 H22 cells into the liver of BALB/c mice. Three days post tumor inoculation, mice were divided randomly into four groups: (a) PBS (i.v.), (b) OCA 20 mg/kg (*p.o.*), (c) NE (i.v.), (d) OCA-NE 20 mg/kg (i.v., Fig. 5A). At the end of the experiment, mice liver was excised, tumor and liver weight were recorded, and the tumor/

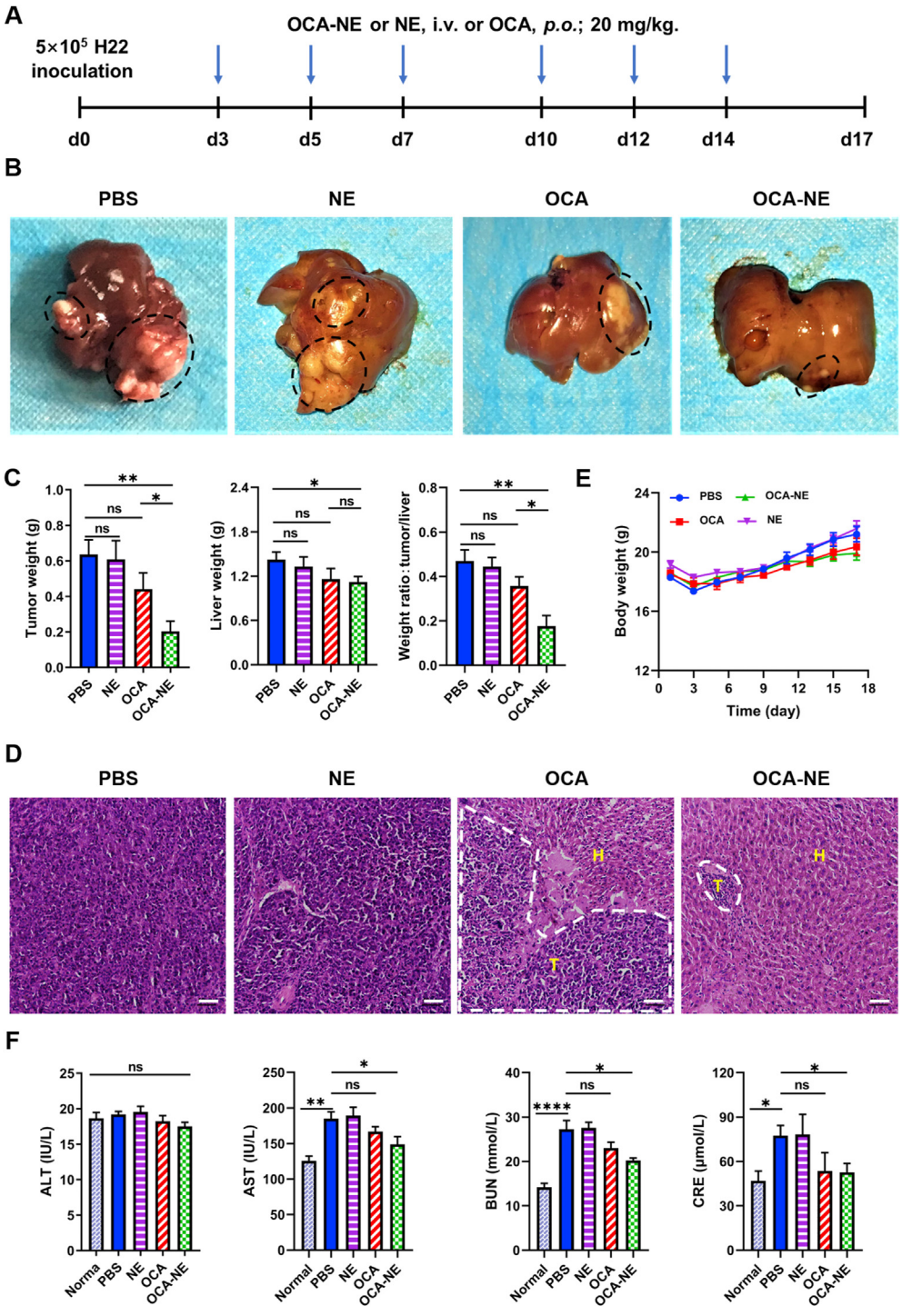

Figure 5 Tumor inhibition study of OCA-NE in orthotopic H22 mice model. (A) Treatment scheme. Mice were sacrificed on day 17 after indicated treatments. d represent for day. (B) Representative photos of livers after receiving PBS (i.v.), NE (i.v.), OCA (*p.o.*) and OCA-NE (i.v.) treatment. The livers were harvested at the end of experiment. The tumors were outlined with black dotted line. H represent hepatocytes, T represent tumor cells. (C) Tumor weight, liver weight and tumor/liver weight ratios after different treatments over time. Data are shown as mean ± SEM ($n = 7$ for NE, OCA and OCA-NE group; $n = 8$ for PBS group). $^{ns}P>0.05$, $^{*}P < 0.05$, $^{**}P < 0.01$, (D) Representative H&E images of tumor sections of different group. The scale bar represents 50 μm. The tumors were outlined with white dotted line. (E)Tumor weight variations of each treatment group over time. Data represent mean ± SEM ($n = 6$). (F)Serum levels of aspartate aminotransferase (AST), alanine aminotransferase (ALT), blood urea nitrogen (BUN) and creatinine (CRE) in mice after treatment and normal mice. Data are shown as mean ± SEM ($n = 3$ for normal group, $n = 4$ for NE, OCA and OA-NE group). $^{ns}P>0.05$, $^{*}P < 0.05$, $^{**}P < 0.01$, $^{***}P < 0.001$.

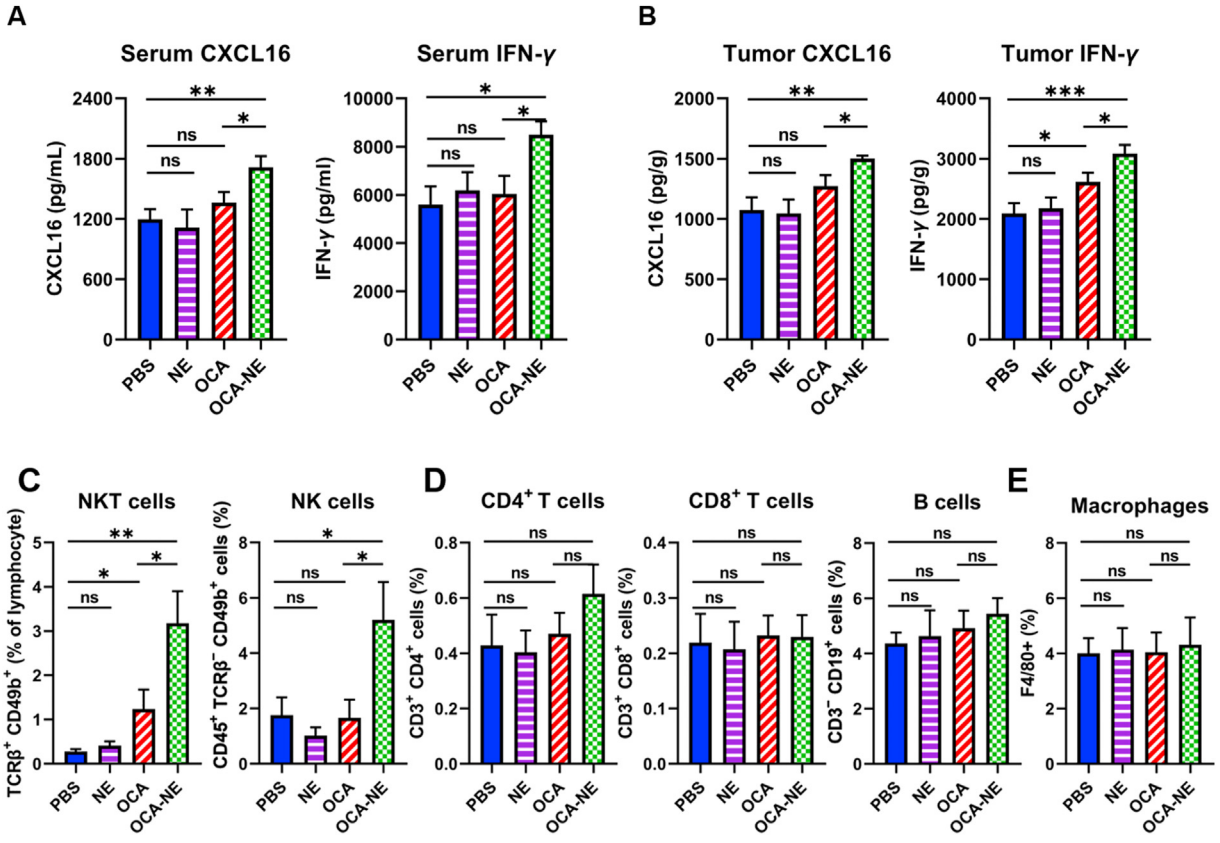

Figure 6 Immune analysis of serum and liver tumor after various treatments. (A) CXCL16 and IFN-γ concentrations in serum. Data are shown as mean ± SEM ($n = 5$). (B) CXCL16 and IFN-γ concentrations in tumors. Data are shown as mean ± SEM ($n = 8$). (C) and (D) Proportions of tumor-infiltrating NKT cells, NK cells, $CD4^+$ T cells, $CD8^+$ T cells and B cells. Data are shown as mean ± SEM, ($n = 7$ for NE; $n = 8$ for PBS, OCA and OCA-NE group). (D) Proportions of tumor-infiltrating macrophages. Data are shown as mean ± SEM, ($n = 7$). $^{ns}P>0.05$, $^{*}P < 0.05$, $^{**}P < 0.01$, $^{***}P < 0.001$.

liver weight ratio was also calculated. As shown in Fig. 5B and C, OCA-NE group had the lighter tumor and liver weight than free OCA group. In addition, the livers of OCA-NE group had the smallest tumor percentage compared with other groups. Furthermore, the tumor suppression rate (TSR%) was 68% in mice on the OCA-NE treatment, which was notably higher than that in free OCA group (30%, $P < 0.05$). These results reveal that OCA-NE presents remarkable antitumor efficacy as compared to the free OCA group.

The antitumor effect was further confirmed by histological analysis at the end of the experiment. The liver tumors were collected and stained with H&E for pathology analysis. As shown in Fig. 5D, untreated and free OCA-treated liver tumor exhibite large nuclei and more chromatin. However, normal and clear hepatic cell morphology were observed in pathological section of OCA-NE treated group, and the chromatin of tumors was concentrated and pyknotic or absent outside the cellular, indicating that OCA-NE treatment group showed better antitumor efficacy compared with free OCA drug. Mice body weight changes were recorded as a surrogate for the adverse effects of the drugs. In the first 7 days after drug administration, no serve body weight loss (>10%) was observed in mice (Fig. 5E). To further visualize the *in vivo* safety of OCA-NE, blood biochemical parameters were examined after 2-weeks of treatment. Owing to the acute hepatic injury and kidney injury caused by tumor lesions, serum AST, BUN, and CRE levels were significantly increased in the H22-bearing mice in the PBS group compared with normal mice (Fig. 5F). Mice receiving OCA-NE treatment showed significantly decreased activities of serum AST, BUN, and CRE levels compared with other treated groups, which might be attributed to reducing tumor burden efficiently after OCA-NE treatment. Theses safety investigations evidenced that the designed OCA-NE was safe and could improve liver and renal function in H22 tumor-bearing mice. In summary, our experimental results confirmed the antitumor effect of OCA against HCC *in vivo* and that precise and 'targeted' delivery of OCA through nanoapproach is necessary in treating orthotopic HCC-bearing mice at a safe and effective therapeutic dosage.

3.8. *In vivo immunity analysis after OCA-NE treatment*

The immune response of after OCA and OCA-NE treatment was investigated. Firstly, the serum and tumoral cytokines including CXCL16 and IFN-γ were determined. The secretion of CXCL16 from LSECs contributes to recruitment of NKT cells to the liver (by interacting with the CXCR6 on NKT cells), while NKT cells regulate the innate and adaptive immunity *via* production of a variety of cytokines including IFN-γ[45,46]. As shown in Fig. 6A and B, both serum and tumoral CXCL16 and IFN-γ levels were much increased after OCA-NE treatment, while free OCA did not induce significant changes. The cytokine secretion results revealed that OCA-NE triggered enhanced immune response compared with free OCA administration, which may be attributed to the precise delivery of OCA to LSECs *via* the nanoapproach. Liver H22 tumors were collected and processed into single cell

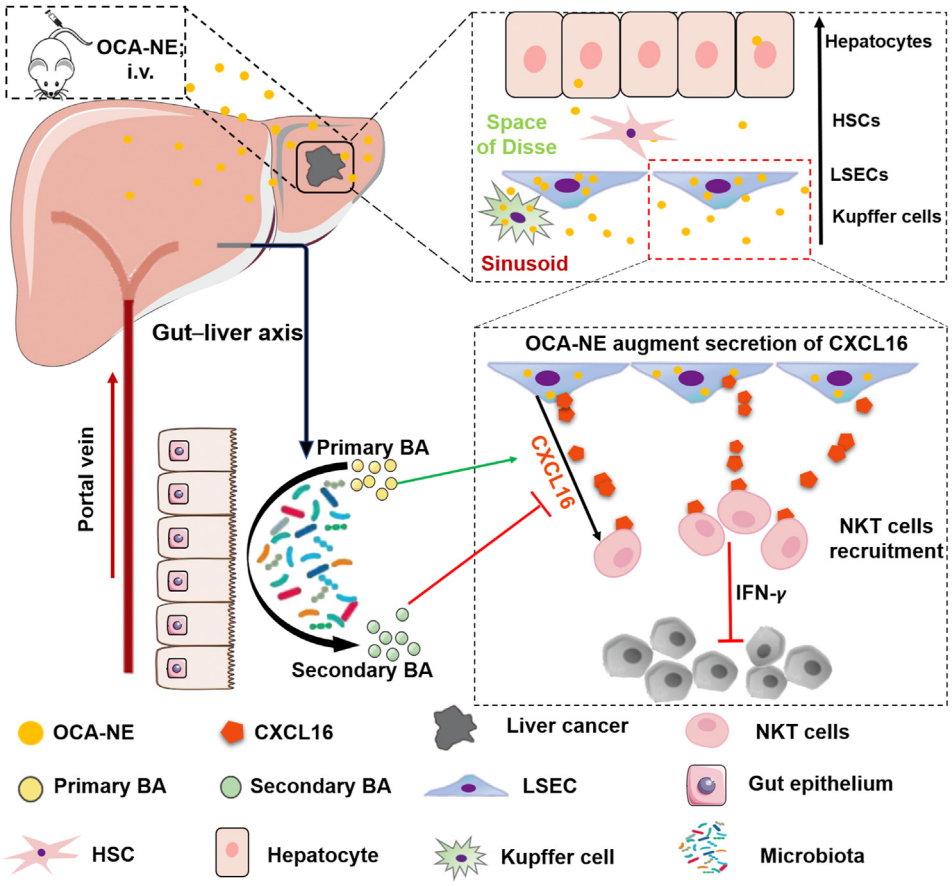

Scheme 1 Mechanism of OCA-NE in precisely manipulating LSECs and NKT cells for liver cancer immunotherapy. The injected OCA-NE accumulates in mouse liver and especially in the LSEC cells, promoting secretion of CXCL16 and recruitment of NKT cells to the tumor, which further inhibit liver tumor growth through secretion of IFN-γ.

suspensions at the end of treatment for flow cytometry analysis. As shown in Fig. 6C–E, OCA-NE treatment resulted in significant increase in NKT and NK cells in the H22 tumor, while no much changes in $CD4^+$ T cells, $CD8^+$ T cells, B cells and macrophages (gating strategy shown in Supporting Information Fig. S5). This is in consistent with previous reports that primary bile acids mainly stimulate NKT cell-mediated immunity in the liver for cancer control[25]. In addition, owing to the precise and 'targeted' delivery of OCA to LSECs in NE, significantly higher hepatic NKT cell levels were determined in OCA-NE group (3.18% of lymphocyte) compared with free OCA group (1.35% of lymphocyte) at the same dosage (Fig. 6B), indicating stronger cellular anti-tumor immune responses induced by OCA-NE than free OCA. Taken together, these data clearly demonstrated that OCA-NE treatment caused augmented secretion of CXCL16 by LSECs, which resulted in enhanced accumulation of NKT cells in liver tumor and effective suppression of liver tumor growth.

4. Conclusions

In this study, a new evidence was provided for the anticancer effect of OCA against liver cancer *in vivo*. OCA was demonstrated to be capable of regulating CXCR6/CXCL16-dependent accumulation of hepatic NKT cells and antitumor immunity in the liver. Secondly, to enhance the antitumor efficacy and overcome the defects of large dosage of OCA, we developed OCA-NE for precisely modulating LSECs for liver immune microenvironment management. *In vivo* biodistribution study showed that OCA-NE mainly accumulate in the liver and a significant amount was delivered to the LSECs, thus resulting in significantly enhanced secretion of CXCL16 and subsequent recruitment of NKT cells to the liver tumor. Our designed OCA-NE represents a novel and promising therapeutic option for liver cancer, and the precise delivery concept should inspire other strategies for using nanoparticles to manipulate LSECs for cancer therapy.

Acknowledgments

This work was financially supported by the National Natural Science Foundation of China (51673189, 51973215, 51833010 and 51520105004), Ministry of Science and Technology of China (Project 2018ZX09711003-012), and the Program of Scientific Development of Jilin Province (20170101100JC, 20180520207JH, and 20190103112JH, China). Leaf Huang is supported by NIH grant CA198999 (USA).

Author contributions

Wantong Song and Xuedong Fang designed the research. Guofeng Ji carried out the experiments and performed data analysis. Lushun Ma, Haochen Yao, Sheng Ma, Xinghui Si, Yalin Wang, Xin Bao and Lili Ma participated part of the experiments.

Fangfang Chen, Chong Ma, Leaf Huang and Wantong Song provided experimental drugs and quality control. Guofeng Ji wrote the manuscript. Fangfang Chen, Leaf Huang, Xuedong Fang and Wantong Song revised the manuscript. All of the authors have read and approved the final manuscript.

Conflicts of interest

The authors have no conflicts of interest to declare.

Appendix A. Supporting information

Supporting data to this article can be found online at https://doi.org/10.1016/j.apsb.2020.09.004.

References

1. Bray F, Ferlay J, Soerjomataram I, Siegel RL, Torre LA, Jemal A. Global cancer statistics 2018: GLOBOCAN estimates of incidence and mortality worldwide for 36 cancers in 185 countries. *CA Cancer J Clin* 2018;**68**:394−424.
2. Chen WQ, Li H, Sun KX, Zheng RS, Zhang SW, Zeng HM, et al. Report of cancer incidence and mortality in China, 2014. *Chin J Oncol* 2018;**40**:5−13.
3. Chen WQ, Sun KX, Zheng RS, Zeng HM, Zhang SW, Xia CF, et al. Cancer incidence and mortality in China, 2014. *Chin J Oncol* 2018;**30**:1−12.
4. Torre LA, Bray F, Siegel RL, Ferlay J, Lortet-Tieulent J, Jemal A. Global cancer statistics, 2012. *CA Cancer J Clin* 2015;**65**:87−108.
5. Song TJ, Ip EW, Fong Y. Hepatocellular carcinoma: current surgical management. *Gastroenterology* 2004;**127**:S248−60.
6. Forner A, Reig M, Bruix J. Hepatocellular carcinoma. *Lancet* 2018;**391**:1301−14.
7. Fu J, Wang HY. Precision diagnosis and treatment of liver cancer in China. *Cancer lett* 2018;**412**:283−8.
8. Wang YL, Yu HY, Zhang DW, Wang GY, Song WT, Liu YM, et al. Co-administration of combretastatin A4 nanoparticles and sorafenib for systemic therapy of hepatocellular carcinoma. *Acta Biomater* 2019;**92**:229−40.
9. Forner A, Gilabert M, Bruix J, Raoul JL. Treatment of intermediate-stage hepatocellular carcinoma. *Nat Rev Clin Oncol* 2014;**11**:525−35.
10. Llovet JM, Ricci S, Mazzaferro V, Hilgard P, Gane E, Blanc JF, et al. Sorafenib in advanced hepatocellular carcinoma. *N Engl J Med* 2008;**359**:378−90.
11. Chan SL, Yeo W, Mo F, Chan AWH, Koh J, Li L, et al. A phase 2 study of the efficacy and biomarker on the combination of transarterial chemoembolization and axitinib in the treatment of inoperable hepatocellular carcinoma. *Cancer* 2017;**123**:3977−85.
12. Cheng AL, Kang YK, Chen Z, Tsao CJ, Qin S, Kim JS, et al. Efficacy and safety of sorafenib in patients in the Asia–Pacific region with advanced hepatocellular carcinoma: a phase III randomised, double-blind, placebo-controlled trial. *Lancet Oncol* 2009;**10**:25−34.
13. Zhu YJ, Zheng B, Wang HY, Chen L. New knowledge of the mechanisms of sorafenib resistance in liver cancer. *Acta Pharmacol Sin* 2017;**38**:614−22.
14. Song WT, Musetti SN, Huang L. Nanomaterials for cancer immunotherapy. *Biomaterials* 2017;**148**:16−30.
15. Song WT, Shen LM, Wang Y, Liu Q, Goodwin TJ, Li JJ, et al. Synergistic and low adverse effect cancer immunotherapy by immunogenic chemotherapy and locally expressed PD-L1 trap. *Nat Commun* 2018;**9**:2237.
16. Ringelhan M, Pfister D, O'Connor T, Pikarsky E, Heikenwalder M. The immunology of hepatocellular carcinoma. *Nat Immunol* 2018;**19**:222−32.
17. Prieto J, Melero I, Sangro B. Immunological landscape and immunotherapy of hepatocellular carcinoma. *Nat Rev Gastroenterol Hepatol* 2015;**12**:681−700.
18. Qin SK, Ren ZG, Meng ZQ, Chen ZD, Chai XL, xiong JP, et al. Camrelizumab in patients with previously treated advanced hepatocellular carcinoma: a multicentre, open-label, parallel-group, randomised, phase 2 trial. *Lancet Oncol* 2020:30011−5.
19. El-Khoueiry AB, Sangro B, Yau T, Crocenzi TS, Kudo M, Hsu C, et al. Nivolumab in patients with advanced hepatocellular carcinoma (CheckMate 040): an open-label, non-comparative, phase 1/2 dose escalation and expansion trial. *Lancet* 2017;**389**:2492−502.
20. Gao B, Radaeva S, Park O. Liver natural killer and natural killer T cells: immunobiology and emerging roles in liver diseases. *J Leukoc Biol* 2009;**86**:513−28.
21. Bricard G, Cesson V, Devevre E, Bouzourene H, Barbey C, Rufer N, et al. Enrichment of human $CD4^+$ V(alpha)24/Vbeta11 invariant NKT cells in intrahepatic malignant tumors. *J Immunol* 2009;**182**:5140−51.
22. Szabo G. Gut–liver axis in alcoholic liver disease. *Gastroenterology* 2015;**148**:30−6.
23. Dapito DH, Mencin A, Gwak GY, Pradere JP, Jang MK, Mederacke I, et al. Promotion of hepatocellular carcinoma by the intestinal microbiota and TLR4. *Canc Cell* 2012;**21**:504−16.
24. Song WT, Tiruthani K, Wang Y, Shen LM, Hu MY, Dorosheva O, et al. Trapping of lipopolysaccharide to promote immunotherapy against colorectal cancer and attenuate liver metastasis. *Adv Mater* 2018;**30**:e1805007.
25. Ma C, Han MJ, Heinrich B, Fu Q, Zhang QF, Sandhu M, et al. Gut microbiome-mediated bile acid metabolism regulates liver cancer *via* NKT cells. *Science* 2018;**360**. eaan5931.
26. Postler TS, Ghosh S. Understanding the holobiont: how microbial metabolites affect human health and shape the immune system. *Cell Metab* 2017;**26**:110−30.
27. Trivedi PJ, Hirschfield GM, Gershwin ME. Obeticholic acid for the treatment of primary biliary cirrhosis. *Expet Rev Clin Pharmacol* 2016;**9**:13−26.
28. Kowdley KV, Luketic V, Chapman R, Hirschfield GM, Poupon R, Schramm C, et al. A randomized trial of obeticholic acid monotherapy in patients with primary biliary cholangitis. *Hepatology* 2018;**67**:1890−902.
29. Manne V, Kowdley KV. Obeticholic acid in primary biliary cholangitis: where we stand. *Curr Opin Gastroenterol* 2019;**35**:191−6.
30. Geissmann F, Cameron TO, Sidobre S, Manlongat N, Kronenberg M, Briskin MJ, et al. Intravascular immune surveillance by $CXCR6^+$ NKT cells patrolling liver sinusoids. *PLoS Biol* 2005;**3**:e113.
31. Zhou H, Fan ZY, Li PY, Deng JJ, Arhontoulis DC, Li CY, et al. Dense and dynamic polyethylene glycol shells cloak nanoparticles from uptake by liver endothelial cells for long blood circulation. *ACS Nano* 2018;**12**:10130−41.
32. Song WT, Das M, Chen XS. Nanotherapeutics for immuno-oncology: a crossroad for new paradigms. *Trends Cancer* 2020;**6**:288−98.
33. Rai VK, Mishra N, Yadav KS, Yadav NP. Nanoemulsion as pharmaceutical carrier for dermal and transdermal drug delivery: formulation development, stability issues, basic considerations and applications. *J Control Release* 2018;**270**:203−25.
34. Xu HY, Liu CS, Huang CL, Chen L, Zheng YR, Huang SH, et al. Nanoemulsion improves hypoglycemic efficacy of berberine by overcoming its gastrointestinal challenge. *Colloids Surf B Biointerfaces* 2019;**181**:927−34.
35. Attia YM, Tawfiq RA, Ali AA, Elmazar MM. The FXR agonist, obeticholic acid, suppresses HCC proliferation & metastasis: role of IL-6/STAT3 signalling pathway. *Sci Rep* 2017;**7**:12502.

36. Di Matteo S, Nevi L, Costantini D, Overi D, CarpinoG Safarikia S, et al. The FXR agonist obeticholic acid inhibits the cancerogenic potential of human cholangiocarcinoma. *PLoS One* 2019;**14**: e0210077.
37. Hu CM, Zhang L, Aryal S, Cheung C, Fang RH, Zhang L. Erythrocyte membrane-camouflaged polymeric nanoparticles as a biomimetic delivery platform. *Proc Natl Acad Sci U S A* 2011;**108**: 10980−5.
38. Zhao XY, Liu XY, Zhang PC, Liu YR, Ran W, Cai Y, et al. Injectable peptide hydrogel as intraperitoneal triptolide depot for the treatment of orthotopic hepatocellular carcinoma. *Acta Pharm Sin B* 2019;**9**: 1050−60.
39. Tavoloni N. The intrahepatic biliary epithelium: an area of growing interest in hepatology. *Semin Liver Dis* 1987;**7**: 280−92.
40. Daoust R, Cantero A. The numerical proportions of cell types in rat liver during carcinogenesis by 4-dimethylaminoazobenzene (DAB). *Cancer Res* 1959;**19**:757−62.
41. Park JK, Utsumi T, Seo YE, Deng Y, Satoh A, Saltzman WM, et al. Cellular distribution of injected PLGA-nanoparticles in the live. *Int J Nanomed* 2016;**12**:1365−74.
42. Shetty S, Lalor PF, Adams DH. Liver sinusoidal endothelial cells—gatekeepers of hepatic immunity. *Nat Rev Gastroenterol Hepatol* 2018;**15**:555−67.
43. Talmadge JE, Singh RK, Fidler IJ, Raz A. Murine models to evaluate novel and conventional therapeutic strategies for cancer. *Am J Pathol* 2007;**170**:793−804.
44. Wang QL, Zhang P, Li ZM, Feng XR, Lv CY, Zhang HY, et al. Evaluation of polymer nanoformulations in hepatoma therapy by established rodent models. *Theranostics* 2019;**9**:1426−52.
45. Gollnick SO, Vaughan L, Henderson BW. Generation of effective antitumor vaccines using photodynamic therapy. *Cancer Res* 2002;**62**: 1604−8.
46. Korbelik M, Sun J, Cecic I. Photodynamic therapy-induced cell surface expression and release of heat shock proteins: relevance for tumor response. *Cancer Res* 2005;**65**:1018−26.